HIGH QUALITY LASER MICROMACHINING OF SILICON: A CRYSTALLOGRAPHIC COMPARISON OF PROCESS RESULTS ACHIEVED WITH STATE-OF-THE-ART TRIPLED ND:YAG AND IR LASERS

Paper M1101

Claudio Ferrari [1], Lucia Nasi[1], Werner Wiechmann[2], Sergio Pelegrino[3]

[1] Istituto IMEM CNR, Parco Area delle Scienze 37/A, 43010 Parma, Italy
[2] JDSU Corporation, 430 North McCarthy Boulevard, Milpitas, CA 95035, U.S.A.
[3] LaserPoint srl, Via Burona 51, 20090 Vimodrone, Italy

Abstract

The ability to cut, scribe, and drill holes and slots in silicon material is of great interest for many applications in the microelectronics and semiconductor industry. We investigated the use of a Q-switched frequency-tripled Nd:YAG laser for rapid micromachining of silicon and compared the results to results achieved with a pulsed fiber laser operating near 1060nm. Cutting, drilling, marking and surface ablation were performed by direct writing using a high-speed x-y galvano-mechanical beam positioner equipped with a telecentric lens focusing system and a high precision x-y-z stage.

This paper focuses on circular and linear cutting experiments on "thick" silicon wafers, i.e. wafers with a thickness of 440 μm and above.

The sample morphology was studied by scanning electron microscopy; the results indicate 8-10 times larger surface roughness on the IR processed samples.

We also applied X-ray double-crystal topography to analyse the defects and local strain induced by the two laser processes. The topographs show remarkable differences between the cuts generated by the UV laser and the cuts produced by the IR laser.

Our data reveals the capabilities and limitations of both laser types for micromachining in different silicon wafers and helps the user select a laser for a specific process. The results demonstrate the advantages of the short-wavelength laser for damage-free micromachining of silicon.

Introduction

Motivated by the need for a reduced via size, diode-pumped multi-watt Q-switched 355-nm lasers were commercialized more than 10 years ago primarily for micro via drilling in printed circuit boards. This new generation of lasers replaced less reliable and maintenance-intensive lamp-pumped Q-switched 355-nm lasers in this application. Initially, the new lasers operated at pulse repetition rates of less than 5 kHz with less than 3 Watts of output power. Driven by the need for increased processing speed, the powers and pulse repetition rates of these lasers were scaled to more than 20 W and 100 kHz over the last 10 years [1]. Due to these advances, the lasers also made inroads into other high-precision micromachining applications such as cutting and drilling of silicon wafers, scribing of low-k dielectrics and Sapphire substrates, micromachining of slots in silicon wafers and scribing and drilling in thin and thick-film solar cells.

In the above applications the end user demands a low maintenance and a reliability that exceeds 10,000 hours of operation without failure. At the same time, it is critical that the laser provides a near diffraction-limited beam and a stable performance. The latter includes a spatially stable beam profile, stable beam pointing, stable long-term output power and stable pulse-to-pulse energy under various trigger conditions.

The 355-nm laser used in this paper achieves the above requirements through a special side-pumped gain architecture called Direct-Coupled Pump [2] and a patented design for Intracavity Harmonic Generation [3].

The main benefit of the Intracavity Harmonic Generation approach is that it eliminates the need for a periodic shifting of the THG crystal as done in most extra-cavity frequency-converted 355-nm lasers. This enables long-term stable output power and a spatially stable output beam. Another benefit of the Intracavity Harmonic Generation scheme is that it leads to a high pulse-to-pulse energy stability [4].

For generating coherent near IR light cladding-pumped fiber technology has revolutionized the low and high power laser market over the last fifteen

years [5]. Single mode fiber lasers provide an efficient, compact, and reliable solution for micromachining a large variety of materials. Ytterbium fiber lasers operating near 1060 nm deliver good beam quality, a wide operating power range, and high power stability; all these parameters are relevant for a high-quality, high-efficiency cutting process. The high mode quality and small spot size enable cutting of complex features in thin material. True single-mode pulsed fiber lasers with M^2 values below 1.2 and more than 100 W of output power have become commercially available [6]. Operation of these devices in a pulsed mode enables cutting with minimal slag and heat affected zone, which is critical for many micromachining applications. High power densities associated with small spot sizes of the fiber laser also translate into fast cutting with good edge quality. Examples of cutting of semiconductors with pulsed fiber lasers include cutting of silicon wafers for manufacturing of solar cells and cutting of silicon wafers for high-power electronic devices.

Purpose of the Work

The primary purpose of this work is to explore the application limits of state-of-the-art tripled Nd:YAG and IR fiber lasers with respect to cutting and slotting of silicon wafers of different thicknesses.

We target two application areas. The first application is cutting of circular shaped silicon devices with a p-n-p structure in a nested layout. The silicon wafers have a round chip layout after p-n-p junction formation and are cut using a pulsed fiber laser as the laser of choice. The different types of round devices have different diameters with specific electrical parameters. Production of these devices employs silicon wafers with different chip layouts and different thicknesses ranging from 200 to 440 μm. The diameters of the chips vary from 19 to 38 mm. The wafer sizes are 4 and 5 inches and the number of chips on each wafer ranges from 7 to 31.

The second targeted application is the fabrication of high-quality linear slots in silicon wafers that are more than 600 μm thick. State-of-the-art tripled Nd:YAG lasers give superior results in this application with respect to tight control of slot dimensions, good surface finish, the absence or infrequent occurrence of edge chipping, and the low re-deposition/recasting.

Finally, this investigation is intended to highlight the effect of the large difference in absorption between 1064- and 355-nm wavelengths in silicon. The 1064-nm absorption coefficient in silicon is approximately 10^5 times smaller than the equivalent 355-nm absorption coefficient. The low absorption at 1064-nm has a significant thermal impact on the crystallographic structure of the silicon. This reduces the production yield or renders the process infeasible.

Experiments

Laser Systems Used in the Experiments

The experiments were carried out in two different cutting system arrangements:

The first "UV" bench setup includes:

- A Q-switched, diode pumped Nd:YAG laser with more than 10 W average power at 355 nm, TEM_{00}, $M^2 < 1.2$, optimized at 10-30 kHz or
- A Q-switched, diode pumped Nd:YAG laser with more than 10 W average power at 355 nm, TEM_{00}, $M^2 < 1.2$, optimized at 40-80 kHz.
- A high-speed *x-y* galvano-mechanical beam positioner equipped with a telecentric lens focusing system, nominal focal length of 100 mm (and a high precision *x-y-z* stage for accurate sample positioning), automatic self-calibration for temperature compensation and calibration for non-linearity compensation, resulting in estimated repeatability of about 5 microns.

The second "IR" bench setup includes:

- A pulsed fiber laser, 20 and 50 W average power, 1055 nm, TEM_{00}, $M^2 = 1.15$, 20-100 kHz
- A high-speed *x-y* galvano-mechanical beam positioner equipped with an F-Theta lens focusing system, nominal focal length of 100 mm, automatic self-calibration for temperature compensation and calibration for non-linearity compensation, resulting in estimated repeatability of about 5 microns.

X-ray Topography Setup

The samples were investigated using the technique of double crystal x-ray topography [7]. In a typical scheme of double crystal topography a monochromator Ge crystal set at the Bragg condition for the 620 Bragg reflection is used to reflect the $CuK\alpha_1$ line of the Cu anode at a Bragg angle of 59.4° and to produce a parallel x-ray beam several cm^2 wide. To reduce the instrumental broadening and the wavelength dispersion effect, the 531 Bragg

reflection at a Bragg angle of 57.4° with the 531 diffracting planes nearly parallel to the 620 diffraction planes of the monochromator was chosen for the silicon samples. In this condition the rocking curves obtained by rotating the samples in a narrow range near the Bragg angles had a full width at half maximum of nearly 15 arcseconds. The topographs were obtained by putting a radiographic plate on the diffracted beam and by setting the angle of incidence of the x-ray beam on the sample to yield 80% of the peak intensity. The contrast in the topograph is related to bending of the local lattice planes induced by local strain in the crystal [8]. In the chosen setting a local inclination of the lattice planes of 2 arcseconds or a lattice parameter change of $\Delta d/d=6.2x10^{-6}$ gives rise to a 10% variation of the local diffracted intensity. The regions of the topographs showing a darker contrast correspond to areas with higher diffracted intensity.

It is worth noting that the penetration of the x-ray beam in silicon is more than 100 μm for the CuKα radiation, so that the presence of a thin recast layer of non crystalline silicon deposited near the borders does not affect the contrast.

Silicon Wafers Used in the Experiments

Silicon (100) orientation, one side polished, one side etched, 6" diameter, 670 μm thick, undoped.

Silicon (111) orientation, two sides etched, 5" diameter, 440 μm thick, undoped.

Cutting Strategy

The laser beam was moved in a circular trajectory with multiple passes, varying the trajectory diameter by 40 μm steps either pointing outside or inside the device. The linear cut was performed by using a complex beam movement strategy, which will not be described in detail.

Finally, linear cuts were realized on (100) oriented, 670 μm thick silicon with UV and fiber lasers.

List of Experiments

Table 1 lists the different experiments and the parameters used.

Table 1: List of Experiments.

UV Laser, Silicon (100), 670μm, 10mm ∅ Devices				
Sample	Power (W)	Rep Rate (kHz)	Speed (mm/s)	Beam Trajectory
UV#1	13	15	100	To larger radius
UV#2	13	15	100	To smaller radius

UV Laser, Silicon (111), 440μm, 25mm ∅ Devices				
Sample	Power (W)	Rep Rate (kHz)	Speed (mm/s)	Beam Trajectory
UV#3	13	15	180	To larger radius
UV#4	13	15	180	To smaller radius

Fiber Laser, Silicon (100), 670μm, 10mm ∅ Devices				
Sample	Power (W)	Rep Rate (kHz)	Speed (mm/s)	Beam Trajectory
FL#1	45	45	180	Super-imposed
FL#2	45	45	180	To smaller radius
FL#3	45	45	180	To larger radius

UV Laser, Silicon (111), 440μm, 25mm ∅ Devices				
Sample	Power (W)	Rep Rate (kHz)	Speed (mm/s)	Beam Trajectory
FL#4	45	45	180	To smaller radius
FL#5	45	45	180	To smaller radius
FL#6	45	45	180	To larger radius
FL#7	45	45	180	To larger radius

Results

Morphological Characterization, Round Devices

25 mm round devices, 440 μm thick samples: IR laser cutting Samples FL#4 and FL#6 were analyzed. Different SEM perspective- and top- views of the samples showed that the edge contours can be rough, with indentations up to 25 μm (Fig. 1) and chipping defects on the cut exit surface, as clearly shown in Fig. 2. The edge quality is smoother with lower section roughness in samples cut with the laser moving from the center to the periphery of the device.

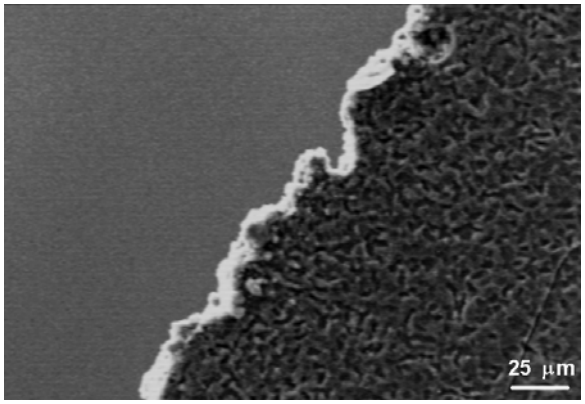

Figure 1: SEM image of the edge contour of sample FL#4, cut exit side.

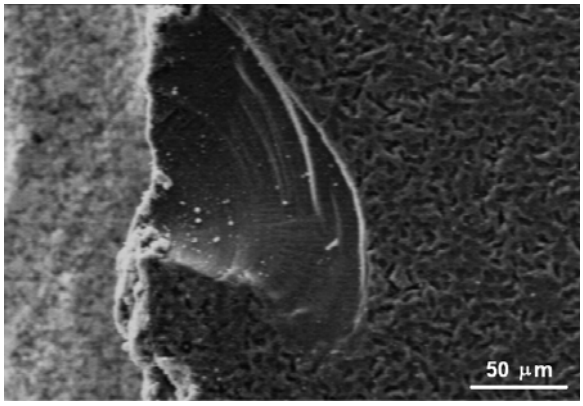

Figure 2: SEM image of a chipping defect along the edge of sample FL#4, cut exit side.

25 mm round devices, 440 μm thick samples: UV laser cutting Samples UV#3 and UV#4 were analyzed. The edges of sample UV#4 have the best quality among all the investigated samples. This device was cut with the laser beam moving from the periphery to the center of the device. The SEM observations in perspective view show that the edges are very smooth, within a range of a few microns (Fig. 3). No chipping effect was visible on the cut exit surface. The section along the cutting path has a very low roughness and is smoother near the cut exit side; here striations with a period of about 9 μm are clearly visible.

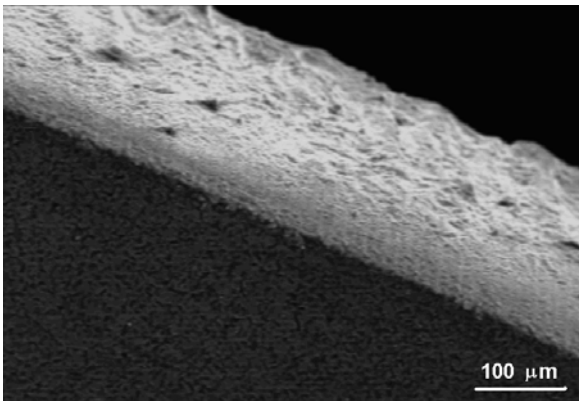

Figure 3: SEM image of a section of sample UV#4, viewed from the cut exit side.

10 mm round devices, 670 μm thick samples: IR laser cutting Sample FL#1, FL#2 and FL#3 were analyzed. The cut edges of all samples are rough with indentations up to 25 μm (Fig. 4). The cut edges of the back-sides are seriously damaged by the presence of large chips which are particularly evident in sample FL#2 (Fig. 5), which was cut with the laser beam moving from the periphery to the center of the device. The morphology features of the sections along the cutting path strongly depend on the direction of the laser beam movement during the cutting process. When the laser makes superimposed rotations (sample FL#1), the section surface is homogeneous throughout the cutting path and reveals rough striations with a period of about 80 μm (Fig. 6). On the contrary, two regions are visible at different depths when the laser beam moves from the periphery to the center (sample FL#2, Fig. 7) or from the center to the periphery (sample FL#3, Fig. 8):

1. A prominent region near the cut-entry surface where re-deposited material is visible and

2. A region near the back side which shows the typical striations.

The cut edge roughness of sample FL#2 is higher than that of sample FL#3 as shown in Fig. 8.

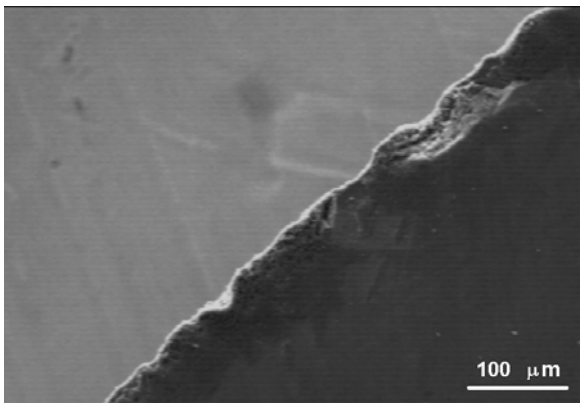

Figure 4: SEM image of the edge contour of sample FL#3, cut exit side.

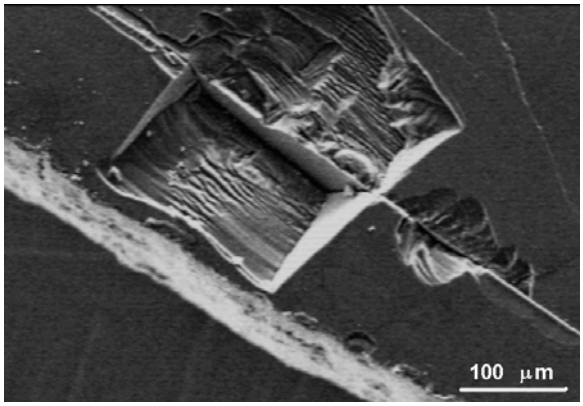

Figure 5: SEM image of a large chip along the edge of sample FL#2, cut exit side.

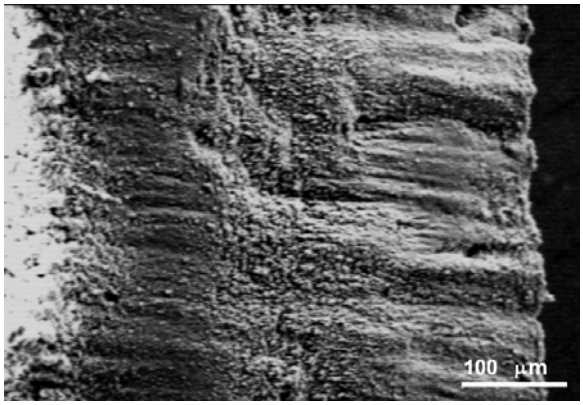

Figure 6: SEM image of the surface along the cutting path of sample FL#1, laser entry side on the left.

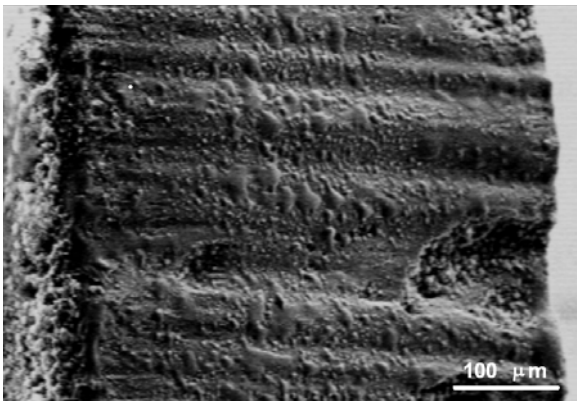

Figure 7: SEM image of the surface along the cutting path of sample FL#2, laser entry side on the left.

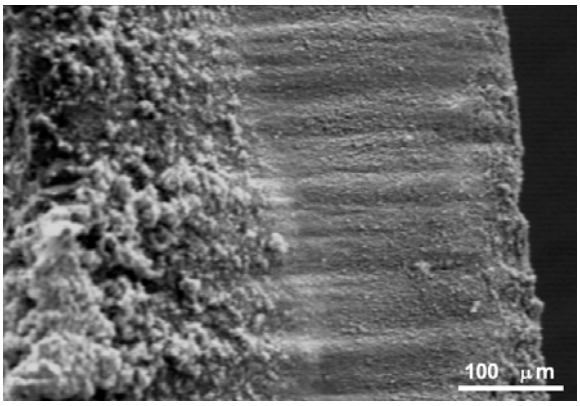

Figure 8: SEM image of the surface along the cutting path of sample FL#3, laser entry side on the left.

10 mm round devices, 670 μm thick samples: UV laser cutting Samples UV#1 and UV#2 were analyzed. The edge contours have indentations up to 15 μm deep and no chipping effect was visible. However, the back-surface shows some residual defects along the edges of the devices in both samples, as shown in Fig. 9 for the UV#1 sample. The cut surface along the laser path of UV#2 sample is rougher than that of UV#1 sample (Fig.10).

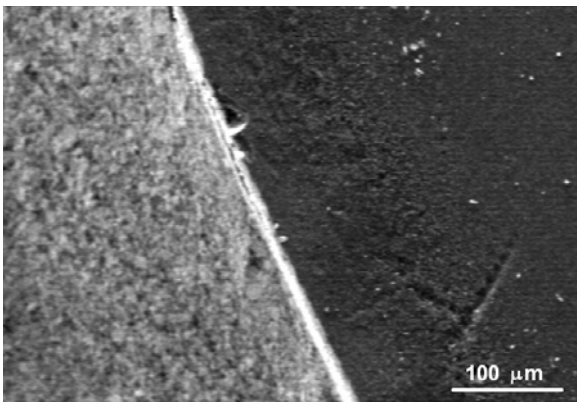

Figure 9: SEM image of the edge contour of sample UV#1, cut exit side.

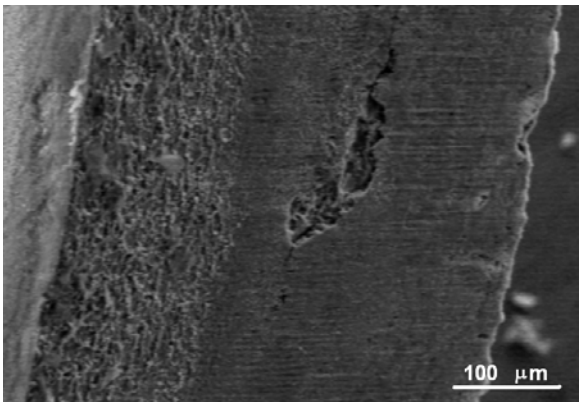

Figure 10: SEM image of the surface along the cutting path of sample UV#1, laser entry side on the left.

X-Ray Topography Characterization, Round Devices

25 mm round devices, 440 μm thick samples Fig. 11 and Fig. 12 show the topographs of 25 mm diameter silicon disks cut from a (111) oriented, 440 μm thick wafer. Sample FL#4 was cut using an IR and sample UV#3 was cut using a UV laser. In both topographs a darker contrast is visible within a range of 100 μm near the border of the sample. This contrast is an indication of the residual strain induced by the cutting process. Assuming that a 10% contrast change is visible by the eye, the contrast arises from zones of the crystal with lattice bending larger than 2 arcseconds and is largest near the border of the samples.

The IR cut sample topograph of Fig. 11 reveals a very irregular border near point A. In this position the apparent border shows a segmented profile with straight lines corresponding to the trace of (100) planes on the (111) surface plane. This is a clear indication of a plastic deformation of the crystal with dislocation gliding on the easy (111) planes for the face centered cubic structure of silicon [9].

Since the plastic deformation is due to movement of dislocations, which is greatly enhanced at higher temperatures [10], we can conclude that the IR cutting process induces larger heat diffusion.

No marked difference was visible between samples cut by increasing the radius of the circular beam trajectory and samples cut by decreasing the radius of the circular beam trajectory.

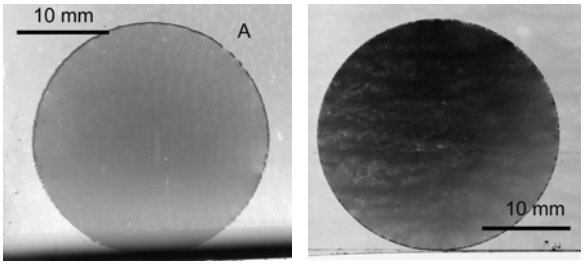

Figure 11 and 12: Double crystal x-ray topographs of silicon disks cut by IR laser (sample FL#4) and UV laser (sample UV#3). The 531 scattering vector has a vertical projection in the picture.

10 mm round devices, 670 μm thick samples Fig. 13 and Fig. 14 show the topographs of 670 μm thick (100) oriented silicon disks cut with the IR laser by moving the beam on the same circle (sample FL#1) and to inner circles (sample FL#2). The images show a variation of the contrast within an area less than 200 μm from the border and dislocation loops are visible at the (011) edges of the wafers. This indicates that the heat flow in the thicker IR machined samples is high enough to permit the movement of dislocations several hundredths of microns inside the sample. The residual strain for the sample cut when the IR beam moves toward inner circles is even worse with the strain penetrating several hundred microns and there is evidence of crack formation near point A in Fig. 14 and a marked plastic deformation at the (011) edges of the sample.

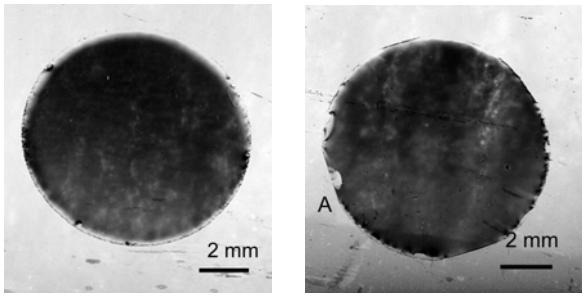

Figure 13 and 14: Double crystal x-ray topographs of 670 mm thick, 10 mm diameter silicon disks (samples FL#1 and FL#2) cut with the IR laser by superimposing the tracks and by moving to inner circles laser respectively. The 531 scattering vector has a vertical projection in the picture.

Fig. 15 and Fig. 16 are topographs of 670 μm thick (100) oriented silicon disks cut with the UV laser by moving the beam toward inner circles (sample UV#2) and toward outer circles (sample UV#1). Both samples exhibit a contrast at the border extending for 150 μm and 100 μm respectively, but the sample in Fig. 15 exhibits a visible small dislocation loop and a more irregular contrast at the border. In contrast, such effects are nearly completely absent in the sample in Fig. 16. This result may be understood if the heat load during the cutting process is considered. Due to the much shorter absorption length of the UV beam in silicon a higher energy density is delivered to the processed volume during the UV cutting process. The heat flow toward the material not directly hit by the laser beam is much lower during the UV process than it is during the IR process.

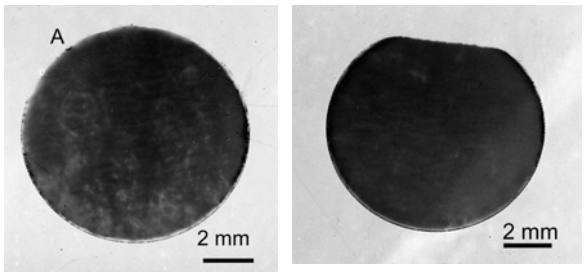

Figure 15 and 16: Double crystal x-ray topographs of 670 mm thick, 10 mm diameter silicon disks cut with the UV laser by moving the beam toward inner circles (sample UV#2) and toward outer circles (sample UV#1). The 531 scattering vector has a vertical projection in the picture.

This heat flow is responsible for the plastic deformation of crystal zones near the cutting zone. By moving the laser beam to the inner radius the heat flows add up extending the range at which dislocation and plastic relaxation may occur.

Preliminary Morphological Characterization, Linear Cuts for Slotting

Fig. 17 shows the results obtained with an optimized linear cutting strategy. The slots were realized on (100) oriented, 670 μm thick silicon with UV and fiber lasers and will be reported in more detail at the conference.

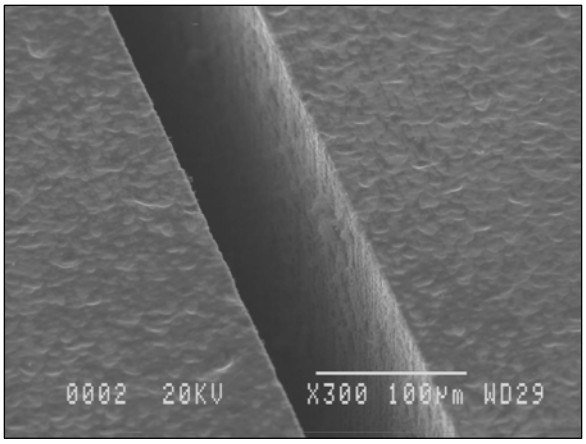

Figure 17: Nearly perfect linear UV laser cut, (100) oriented, 670 μm thick silicon wafer.

Preliminary X-Ray Topography Characterization, Linear Cuts for Slotting

To illustrate the effect of long range strain associated with the IR laser cutting process, Fig. 18 shows the topograph of a (100) oriented wafer in which several internal single cuts were performed.

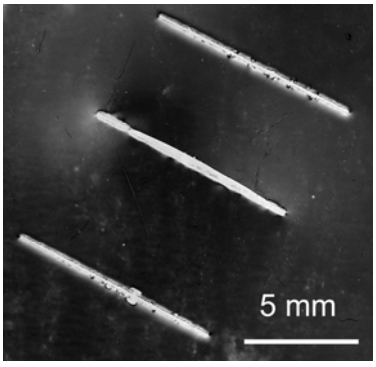

Figure 18: Double crystal x-ray topographs of a 670 μm thick silicon wafer with three parallel cuts produced by the IR fiber laser. The 531 scattering vector has a vertical projection in the picture.

The figure shows three parallel cuts spaced by approximately 5 mm. The strain induced by the cut is especially visible in the central cut in which a contrast variation is visible several mm from the end points of the cut. Small dislocation loops are visible in the first and third cut. Such long range strain has been found responsible for dislocation slip several mm from the cut edges in IR cut samples.

Discussion

Morphological Characterization

For the 25 mm devices, we can conclude that the surface quality obtained by UV lasers is, as expected, better than that the surface quality obtained by IR lasers.

Edge contour indentations decrease from about 25 μm to only a few μm when changing from IR to UV laser cutting. UV laser cutting does not produce chipping effects while IR laser cutting seriously affects the structural properties of the cuts. Also, the cut edge along the UV laser path is significantly smoother than the cut edges along the IR laser path.

For IR laser cutting, the edge quality is better when the laser beam moves from the center to the periphery of the devices, resulting in good surface morphology and acceptable roughness.

For the 10 mm devices we can conclude that the UV laser achieves smoother edge cut contours than the IR laser (25 μm indentations versus 10 μm indentations). Large chips are visible in the IR samples while they are absent in the UV samples. All the cut edge surfaces are very rough except for sample UV#1 which was cut by UV laser with the beam moving from the center to the periphery.

As for IR-laser cutting, no remarkable differences in edge contours were found between the 440 μm and 670 μm thick devices. The IR produced edge contours have indentations up to about 25 μm for both thicknesses.

The use of UV laser enables very smooth edge contours only for the 440 μm samples.

The chipping effect, which is typical for IR-laser cutting, is particularly striking in the 670 μm devices.

As for the roughness of the cut sections, zones with different morphology along the device depth were visible in the 670 μm thick samples for both IR and UV cutting. On the contrary, the cut edges are homogeneous along the device depth in case of the 440 μm-thick samples.

Topography Characterization

The x-ray topography characterization of the laser machined samples indicates the presence of strain extending several hundred microns form the cut border. Such strain is higher for the thicker samples cut by IR laser and may induce plastic deformation mainly along crystal directions which favor the movement of dislocations. The cutting procedure may also influence the residual strain; moving the laser beam to trajectories with smaller radii leads to increased local strain and plastic deformation.

Summary

In conclusion, we have highlighted the application potentials and limits of Q-switched frequency-tripled Nd:YAG lasers and pulsed fiber lasers operating near 1060 nm for rapid micromachining of thick silicon wafers.

In our setup, 440 μm represented the upper wafer thickness limit for fabricating high-quality round devices with the fiber laser while no thickness limitations were found when employing the UV laser.

In case of fiber laser cutting, employing an optimized cutting strategy by moving the heat deposition away from the device-under-process results in a good surface finish and low associated crystallographic strain. Here, the results are comparable to results achieved with the UV laser.

The associated thermal mechanism, including comprehensive 3D modeling will be shown in detail at the conference. This includes compressive stress in case on inward movement of the laser beam with resulting higher process time and increased chipping in case of the optimized process with outward movement of the laser beam.

The UV process leads to very high quality cuts with respect to morphology and crystallography, and achieves a low surface roughness and chip-free edges on wafers as thick as 670 μm.

Nevertheless, even with the UV laser a more sophisticated strategy has to be employed to realize truly damage-free structures. A comprehensive report will be published elsewhere.

Acknowledgements

The author would like to thank G. Salviati (IMEM) and M. Caldironi (LaserPoint) for continuous support and discussion.

References

[1] Wang, C., Wang, G.Y., Hicks, A., Dudley, D., Pang, H. & Hodgson, N. (2006) High-Power Q-Switched TEM_{00} Mode Diode-Pumped Solid State Lasers with > 30W Output Power at 355nm, Proceedings of SPIE, 6100, 335-348.

[2] Kmetec, J. (1998) Solid-state laser with trapped pump light, U. S. Patent 5774488.

[3] Grossman, W. & Henrie, J. (1998) Third-harmonic Generator with uncoated Brewster-cut dispersive Output Facet, U. S. Patent 5850407.

[4] Arbore, M., Balsley, D. Morehead, J., Adams, F., Wiechmann, W., Kmetec, J., Zhou, Y. & Grossman, W. (2005) Measurement Techniques for Laser Parameters Relevant to Materials Processing, Proceedings of Photonics West, San Jose, California, USA, 5713, 402-409.

[5] Schoenfelder, A. (1999) Fiber lasers address micromachining methods, Laser Focus World (June).

[6] Dominc, V., MacCormack, S., Waarts, R., Sanders, S., Bicknese, S., Dohle, R., Wolak, F., Yeh, P.S. & Zucker, E. (1999) 110 W fiber laser, Conference on Lasers an Electro-Optics, Tech. Digest Paper CPD26.

[7] Jenichen, B., Köhler, R. & Möhling, W. (1985) Double Crystal Topography Compensating for the Strain in Processed Samples, Phys. Status Solidi, 89, 79-87.

[8] Hart, M. (1981) Bragg Angle Measurement and Mapping, Journal of Crystal Growth, 55, 409-427.

[9] Hull, D. & Bacon, D.J. (1984) Introduction to Dislocations, 37, Pergamon Press.

[10] Patel, J.R., Testardi, L.R. & Freeland, P.E. (1976) Electronic Effects on Dislocation Velocities in Heavily Doped Silicon, Phys. Rev. B, 13, 3548.

Meet the Authors

Dr. Claudio Ferrari is a Senior Researcher at the IMEM Institute of National Research Council (CNR) in Parma, Italy.

Dr. Lucia Nasi is a Researcher at the IMEM Institute of National Research Council (CNR) in Parma, Italy.

Werner Wiechmann is Product Line Manager at JDSU in Milpitas, California/U.S.A.

Sergio Pellegrino is partner at LaserPoint in Vimodrone, Italy. He is managing the Laser Marking and Micromachining activity.